JOURNAL OF CATALYSIS 157, 436–449 (1995)

Rh_4 Carbonyl Clusters Coordinated with Tris(Hydroxymethyl)phosphine Grafted onto SiO_2 Surfaces and Structural Control of Active Sites in Gas-Phase Olefin Hydroformylation Reactions

Takafumi Shido,* Takumi Okazaki,*,† and Masaru Ichikawa*,[1]

*Catalysis Research Center, Hokkaido University, Kita-ku, Sapporo 060; and †Arakawa Chemical Industries, Ltd., Tsurumi-ku, Osaka 538, Japan

Received March 14, 1995; revised July 31, 1995; accepted August 3, 1995

The structure of attached $Rh_4(CO)_{12}$ on tris(hydroxymethyl)-phosphine ($P(CH_2OH)_3$,THP)-modified silica was investigated by EXAFS and IR spectroscopy. The catalytic behavior of the Rh_4 carbonyl cluster coordinated with THP ligands anchored on $SiO_2(P(CH_2OH)_{3-x}(CH_2OSi)_x$ (x = 1, 2)) in gas-phase hydroformylation reactions was investigated. The number of THP ligands coordinating to the Rh_4 cluster depended on the loading of THP. Rh_4 clusters on SiO_2 loaded with 6.2 wt% THP, on which the average distance of P atoms of the neighboring THP was 8 Å, were coordinated by two THP ligands, and the Rh_4 clusters were distorted. Rh_4 clusters on SiO_2 loaded with 1.6 wt% THP, on the other hand, were coordinated by one THP ligand and the clusters were not distorted. The attached cluster was active for olefin hydroformylation reaction. The reaction rate of hydroformylation on this catalyst was comparable to that on Wilkinson catalyst in solution. The distorted Rh_4 framework, which is coordinated by two THP, was much more active in hydroformylation reactions than was that of monosubstituted clusters of THP/SiO_2 or $Rh_4(CO)_{10}(THP)_2$ in solution. *In situ* IR spectroscopy and EXAFS revealed that a reversible coordination of CO ligands attached to the Rh_4 cluster was associated with the selective hydroformylation reaction. In the hydroformylation atmosphere, the Rh_4 cluster is almost saturated by CO ligands and effectively suppressed the hydrogenation reaction as a side reaction of hydroformylation. In contrast, under the reaction condition of hydrogenation, CO ligands were removed to increase the reaction rate of hydrogenation. The reversible CO bonding in the surface-grafted Rh_4 site was related to the dynamic control of selective hydroformylation of olefins.

1. INTRODUCTION

Some metal cluster compounds are useful molecular precursors for the rational preparation of active metal centers in heterogeneous catalysis because they have well-defined metal frameworks and metal compositions. Metal clusters grafter onto oxide supports (1–5) and entrapped inside zeolite cages (6, 7) offer opportunities for better understanding of the elementary steps of catalytic reactions and the metal–support interactions in terms of organometallic chemistry. Additionally, well-defined active sites derived from surface-attached metal centers can achieve high activity and selectivity. In general, there is a wide spectrum of metal species in the conventional catalysts which cause the decrease of the catalytic selectivity of the products due to the surface heterogeneity. On the other hand, there are advantages to the uniform distribution of the well-defined metal sites in metal cluster-derived catalysts attached to oxide supports such as SiO_2, Al_2O_3, TiO_2, and ZrO_2 (8). Further, the study of the dynamic behavior of active site structures may become more important because it can provide fundamental understanding of catalysis (3, 9, 10).

In general, two methods are used to attach metal clusters to oxide surfaces. One is direct attachment to the oxide surface using a surface reaction between metal clusters and the oxide surface (11). The other is the attachment of metal clusters to a functionalized oxide surface (11). The former technique is used in cases in which metal clusters react with surface active sites such as surface OH groups to form anchored clusters. The advantage of this method is that it allows the generation of new clusters which do not exist stably in solution. It has been reported that $Os_3(CO)_{12}$, $Ru_3(CO)_{12}$, and $Fe_3(CO)_{12}$ attached to oxide surfaces form $HMe_3(CO)_{11}$–(O–) (*Me* = Os, Ru, Fe) species (3, 12). The latter technique is used to attach metal clusters which did not react with the surface or did not anchor to the surface by the surface reaction. Functionalization of oxide surfaces provides ligands that coordinate metal complexes/clusters strongly and blocks surface-active sites such as acid/base sites and surface OH groups that cause the decomposition

[1] To whom correspondence should be addressed.

0021-9517/95 $12.00

of the complexes and clusters. Numerous studies have been performed on the functionalization of oxide surfaces using organic componds such as phosphine, amine, and other organic compounds and the attachment of metal complexes/clusters to the functionalized oxide (11, 13). In the previous study of the functionalization of the oxide surface the aim was to attach metal clusters in such a manner that their structures remained completely the same as in solution, with flex ligands with a long chain, where one end of the chain was anchored to the surface and the other end coordinated to the cluster. However, by using a rigid ligand with a short chain and by the control of the surface density of the ligand, a fine modification of the cluster framework can be achieved that cannot be achieved by the direct attachment of the cluster to an oxide surface or by the conventional functionalization of the oxide surface. It may be possible to distort the cluster structure to obtain interligand distances slightly longer or shorter than the normal distance.

It is reported that $Rh_4(CO)_{12}$ is unstable and decomposed to $Rh_6(CO)_{16}$ when the cluster is impregnated on the oxide surface directly (14, 15). We reported previously, however, that $Rh_4(CO)_{12}$ was attached on tris(hydroxymethyl)phosphine ($P(CH_2OH)_3$,THP)-modified silica surface with their cluster framework remaining intact and that the attached Rh_4 cluster exhibited the catalytic activity for hydroformylation reaction (16, 17).

In this paper we have used EXAFS and IR in order to characterize Rh_4 carbonyl clusters attached on THP-modified silica, with mono- and disubstitution with phosphine ligands, in terms of the structural deformation of the cluster frameworks said to be associated with catalytic activity. Further, we have investigated the dynamic behavior of the attached Rh_4 carbonyl clusters to manage the catalytic activity and selectivity.

2. EXPERIMENTAL

2.1. Sample Preparation

THP is obtained by the reflux of tetrakis(hydroxymethyl)phosphonium chloride (supplied by Albright & Wilson Ltd.) with NEt_4 (18). $Rh_4(CO)_{12}$ (19), $Rh_6(CO)_{16}$ (20) were synthesized by conventional methods. $Rh_4(CO)_{10}(THP)_2$ was synthesized by mixing tetrahydrofuran (THF) solution of $Rh_4(CO)_{12}$ (2.2×10^{-4} mol) and THF solution of THP (4.4×10^{-4} mol) followed by stirring for 12 h.

The grafting of THP on SiO_2 was performed as follows: ethanol solution of THP was mixed under nitrogen with SiO_2 (Aerosil 200, evacuated at 473 K). Then the ethanol was evaporated at room temperature followed by evacuation at 403 K (THP/SiO_2). Two kinds of THP/SiO_2 were prepared with initial THP loadings of 8.0 (THP/SiO_2(I)) and 2.0 wt% (THP/SiO_2(II)), respectively.

The attachment of Rh clusters/complexes on THP/SiO_2 was performed as follows: a hexane solution of $Rh_4(CO)_{12}$ and $[Rh(CO)_2Cl]_2$ (commercially obtained) and a dichloromethane solution of $Rh_6(CO)_{16}$ were added to THP/SiO_2 support under nitrogen atmosphere and stirred 12 h to complete the carbonyl substitution of rhodium clusters with THP/SiO_2. Then the solvent was evaporated at room temperature ($Rh_4/THP/SiO_2$, $[Rh(CO)_2Cl_2]_2/THP/SiO_2$, and $Rh_6/THP/SiO_2$). The loadings of Rh atoms of Rh clusters attached on THP/SiO_2(I) and THP/SiO_2(II) were 4.5 and 1.0 wt%, respectively.

2.2. Stoichiometry of CO Evolution during Attachment of $Rh_4(CO)_{12}$ on THP/SiO_2

The amount of desorbed CO during attachment of $Rh_4(CO)_{12}$ on THP/SiO_2 was measured as follows. THP/SiO_2 was stirred in hexane using Schlenk's tube sealed by septa rubber. $Rh_4(CO)_{12}$ was added through the rubber by using a shilling and stirred 12 h. The tube is connected to a vacuum line equipped with a gas chromatographer (SHIMADZU GC-8A). Molecular sieve 5A (2 m) was used as a column with the column temperature being 333 K. The amount of CO is calculated from the peak height of CO and the dead volume of the tube and vacuum line.

2.3. XPS Measurement to Determine the Loading of THP

XP spectra were measured with a Kratos XSAM-800. The sample was pressed into a self-supporting wafer and mounted in a chamber (2×10^{-8} Torr). Photoemitted electrons of O 1*s*, C 1*s*, P 2*p*, and Si 2*p* were measured with the wide scan mode. The loading of THP was estimated by the atomic ratio of Si and P.

2.4. IR Spectra

IR spectra were measured using a SHIMADZU IR-4100 spectrometer at room temperature or reaction temperature with a resolution of 2 cm^{-1} and accumulated 100–400 times. The THP/SiO_2(I) was pressed into a self-supporting disk and set in a quartz IR cell which was connected with a vacuum line. The disk was evacuated at 403 K for 3 h. Hexane solution of $Rh_4(CO)_{12}$ was dropped on the THP/SiO_2 under N_2 flow. The absorption of THP/SiO_2 and gas phase was subtracted in each spectrum.

2.5. X-Ray Absorption Spectra

Rh *K*-edge X-ray absorption spectra were measured at Photon Factory BL-10B in the National Institute for High

TABLE 1

Crystallographic Data Characterizing the Reference Compounds and Fourier Transform Ranges Used in the EXAFS Analysis[a]

Sample	Crystallographic data			Fourier transform		
	Shell	C.N.	R(Å)	Δk (Å^{-1})	Δr (Å)	n
Rh foil	Rh–Rh[b]	12	2.68	3.5–18.0	1.7–2.9	3
$HRhCO(PPh_3)_3$	Rh–P[c]	3	2.32	3.5–18.0	1.3–2.4	3
$Mo(CO)_6$	Rh–C[d]	6	2.06	3.5–18.0	0.9–2.0	3
	Rh–O[d]	6	3.21	3.5–18.0	2.0–3.3	3

[a] Notation: C.N., coordination number for absorber–backscatterer pair; R, absorber–backscatterer distance; Δk, limits used for forward Fourier transformation; Δr, limits used for shell isolation (r is distance); n, power of k used for Fourier transformation.
[b] Crystal structure data from Ref. (39).
[c] Crystal structure data from Ref. (40).
[d] Crystal structure data from Ref. (41).

Energy Physics. Positron energy and current in the ring were 2.5 GeV and 340–240 mA, respectively. X-ray adsorption spectra was measured with the transmittance mode. A Si(311) channel cut monochromator was used. The X-ray intensity of I_0 and I were measured in an Ar ion chamber charged at 300 V. The path length of the ion chambers were 17 and 62 cm for I_0 and I, respectively. The sample was mounted in a cell with Kapton (rtm) windows. The thickness of the cell was 15 mm for Rh_4/THP/SiO_2(I) and 80 mm for Rh_4/THP/SiO_2(II).

Analysis of X-ray absorption spectra was carried out using the program EXAFS2 (21). The EXAFS (extended X-ray absorption fine structure) function was extracted by the subtraction of background using the Victreen function and cubic sprain method. The k^3-weighted EXAFS function ($\chi(k) \times k^3$) was Fourier transformed and the Fourier transformed function was filtered and inverse Fourier transformed to k-space. The k-range of the Fourier transform and the R-range of the inverse Fourier transform were 3.5–15 Å^{-1} and 1.3–3.7 Å, respectively. The filtered EXAFS function was fitted by the sum of the calculated EXAFS functions for Rh–Rh, Rh–P, Rh–C, and Rh–O. The calculated EXAFS functions were derived using single scattering plane wave theory (21–23). The fitting parameters were coordination number (C.N.), average absorber–backscatter distance (R), correction of inner potential (ΔE_0), and the difference of Debye–Waller-like factors ($\Delta\sigma$) from those of reference compounds.

The backscattering amplitude and phase shift function were extracted from reference compounds. Table 1 summarizes the crystallographic data of the reference compounds and the Fourier transform range used for EXAFS analysis. The function for Rh–Rh was extracted from the first shell of coordination of the Rh foil. The function for Rh–P was extracted from the contribution of Rh–P to $HRh(CO)(PPh_3)_3$, and those for Rh–C and Rh–O were extracted from the contribution of Mo–C and Mo–O to $Mo(CO)_6$, respectively.

The errors of the evaluated parameters were estimated as follows. The parameters for discussion were fixed around the optimum value and the residual was calculated by optimizing the other parameters. The real value was estimated to exist in the range with a residual smaller than twice the residual at the optimum value.

2.6. *Kinetic Studies*

Catalytic reactions were carried out using a closed circulation reactor with a volume of 270 cm^3. About 30 mg catalyst was used for reaction. The products were analyzed by gas chromatography and mass spectrometry. The columns for gas chromatography were Unibeas A (to separate H_2, CO, C_2H_4) and FFAP (to separate C_2H_5CHO). Helium carrier gas was used with 1.5 kg cm^{-2} pressure and 30 cm^3 min^{-1} flow rate. The column temperature was 343 K.

3. RESULTS AND DISCUSSION

3.1. *State of THP on SiO_2 Surfaces*

Figure 1 shows IR spectra of THP/SiO_2(I) evacuated at the various temperatures. A broad band of ν(OH) was observed at 3300 cm^{-1} and sharp bands of ν(CH) of THP were observed at 2986, 2939, and 2908 cm^{-1} in the spectra. A sharp band at 3747 cm^{-1} due to the isolated surface OH of silica decreased when THP was impregnated on the SiO_2 surface. The intensity of the ν(OH) of hydrogen-bonded OH groups was much stronger than that of ν(CH). This may be caused by the difference in mol absorption coefficients between the ν(OH) of hydrogen-bonded OH and ν(CH). The intensity of hydrogen-bonded OH decreased as evacuation temperature increased from 323 to 403 K, whereas the intensity of ν(CH) remained unchanged.

The P/Si atomic ratios of THP/SiO_2(I) and THP/SiO_2(II) were estimated by XPS analysis to be 3.0×10^{-2} and 8×10^{-3}, respectively. As the escape depth of photoelectrons was several nanometers, the loading derived from XPS analysis was not thought to be very different from the real loading. XPS analysis implies that the loadings of THP on THP/SiO_2(I) and THP/SiO_2(II) were 6.2 and 1.6 wt%, respectively. The loading of THP on THP/SiO_2(I) and THP/SiO_2(II) was slightly decreased by evacuation at 403 K, which may be caused by desorption of THP. About 80% of the THP remained on the SiO_2, which is consistent with the results in Fig. 1.

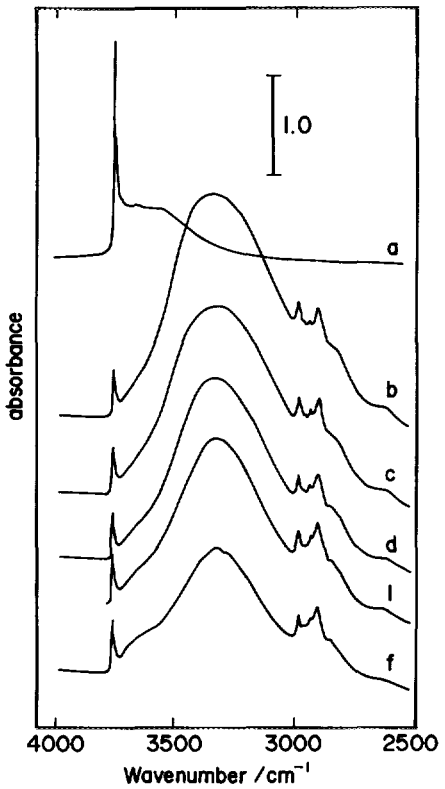

FIG. 1. IR spectra of THP/SiO_2(I). (a) IR spectrum of SiO_2 evaluated at 473 K. (b) After (a), ethanol solution of THP was impregnated on the SiO_2 surface followed by evacuation at 303 K, (c) 323 K, (d) 363 K, (e) 383 K, and (f) 403 K.

As the surface area of used SiO_2, the loading of THP, and the molecular weight of THP were 200 m^2 g^{-1}, 6.2 wt%, and 124, respectively, the density of THP on THP/SiO_2(I) was 1.6 molecules nm^{-2}, which means that the density of the OH groups of impregnated THP was 4.8 groups nm^{-2}. The density of surface OH groups of SiO_2 evacuated at 473 K was 4.7 groups nm^{-2} (11). Hence almost all surface OH groups can interact with THP in the case of THP/SiO_2(I). This is also supported by the IR spectra of the ν(OH) of THP/SiO_2(I), as shown in Fig. 1. When the THP was impregnated onto the SiO_2 evacuated at 473 K, the sharp IR bands at 3747 cm^{-1} which are assigned to isolated OH almost disappeared and broad IR bands appeared at 3300 cm^{-1}, which were assigned to hydrogen-bonded OH.

When the sample was evacuated at increasing temperatures, the IR intensity of hydrogen-bonded OH decreased, whereas ν(CH) at 2986, 2939, and 2908 cm^{-1} remained almost the same in intensity and the intensity of isolated OH at 3747 cm^{-1} did not increase. This result implies that the decrease in hydrogen-bonded OH is not caused by the removal of THP by the evacuation but by the dehydration reaction between surface OH and OH groups of THP, because the intensity of ν(CH) should be decreased and that of isolated OH should be increased when THP is desorbed. The intensity of hydrogen-bonded OH decreased to half of the initial intensity when the sample was evacuated at 403 K. This result suggests that one or two OH groups of THP reacted with surface OH groups as follows:

$$P(CH_2OH)_3 + x(\text{Si–OH}) \rightarrow P(CH_2OH)_{3-x}(CH_2O\text{–Si})_x \quad (x = 1, 2).$$

This analysis explained why 6.2 wt% is the maximum of THP loading. The excess THP molecule that does not interact with surface OH groups may be easy to desorb during evacuation at 403 K.

3.2. *Structure of Attached $Rh_4(CO)_{12}$ on THP/SiO_2*

Figure 2 shows the k^3-weighted EXAFS function ($\chi(k)$) of $Rh_4(CO)_{12}$, $Rh_4(CO)_8(P(OPh)_3)_4$, and Rh_4/THP/SiO_2(I). The k-range of 3.5–15 $Å^{-1}$ for the functions was

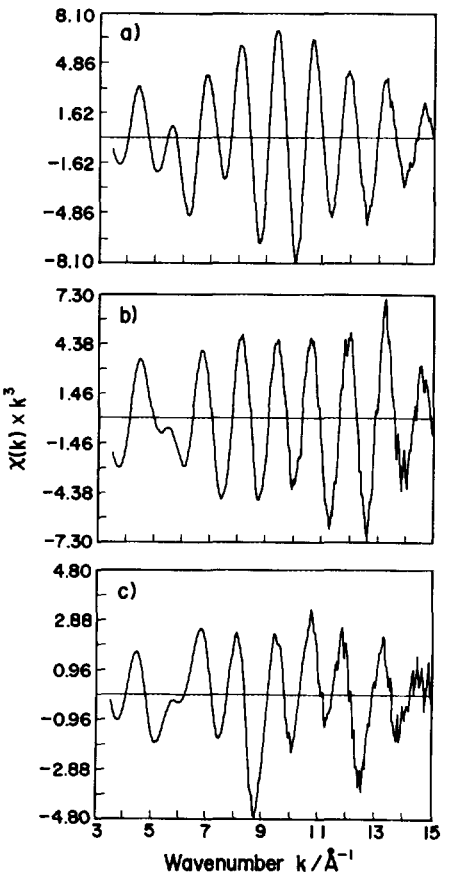

FIG. 2. k^3-weighted Rh K edge EXAFS function ($\chi(k) \times k^3$) of (a) $Rh_4(CO)_{12}$, (b) $Rh_4(CO)_8(P(OPh)_3)_4$, (c) Rh_4/THP/SiO_2(I).

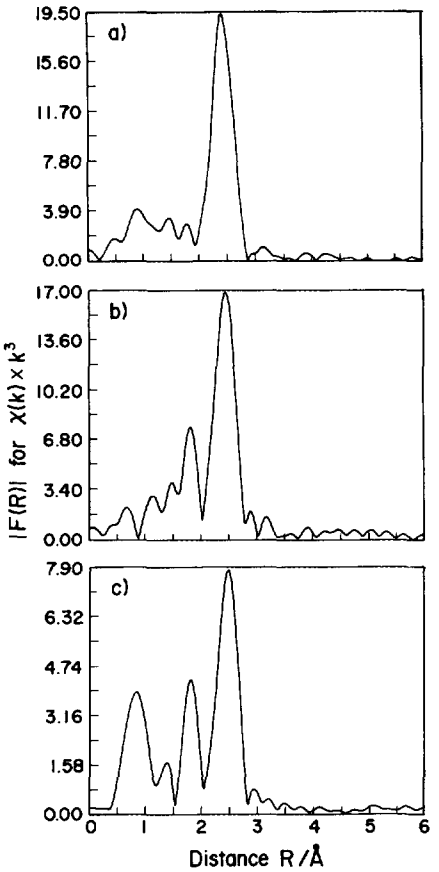

FIG. 3. Fourier transform of k^3-weighted EXAFS function ($\chi(k) \times k^3$) of (a) $Rh_4(CO)_{12}$, (b) $Rh_4(CO)_8(P(OPh)_3)_4$, (c) $Rh_4/THP/SiO_2(I)$.

Fourier transformed as shown in Fig. 3. The phase-shift effect is not corrected for in Fig. 3. In the Fourier transform of $\chi(k) \times k^3$ of $Rh_4(CO)_{12}$ (Fig. 2a) a large peak was observed at 2.4 Å. In the *FT* of $\chi(k) \times k^3$ of $Rh_4(CO)_8(P(OPh)_3)_4$ (Fig. 2b) and $Rh_4/THP/SiO_2(I)$ (Fig. 2c), another peak was observed at 1.8 Å in addition to the peak at 2.4 Å. The *R*-range of 1.3–3.7 Å in Fig. 3 was inverse Fourier transformed and fitted by three waves for $Rh_4(CO)_{12}$ (Rh–Rh, Rh–C, Rh–O) and four waves for $Rh_4(CO)_8(P(OPh)_3)_4$ and attached Rh_4 clusters (Rh–Rh, Rh–P, Rh–C, and Rh–O), as shown in Fig. 4. The inverse Fourier-transformed function was reproduced well by the calculated function.

Table 2 shows structural parameters of $Rh_4(CO)_{12}$, $Rh_6(CO)_{16}$, $Rh_4(CO)_8(P(OPh)_3)_4$, $Rh_4(CO)_{10}(THP)_2$, $Rh_4/THP/SiO_2(I)$, and $Rh_4/THP/SiO_2(II)$, derived by curve fitting of the EXAFS function. The structural parameters of $Rh_4(CO)_{12}$ (24, 25), $Rh_6(CO)_{16}$ (26), and $Rh_4(CO)_8(P(OPh)_3)_4$ (27) are consistent with XRD data. The coordination numbers (C.N.) of Rh–P of $Rh_4(CO)_{10}(THP)_2$, $Rh_4/THP/SiO_2(I)$, and $Rh_4/THP/SiO_2(II)$ were calculated to be 0.44, 0.56, and 0.30, respectively, with an error of ±0.1. This means that the Rh_4 clusters of $Rh_4(CO)_{10}(THP)_2$ and $Rh_4/THP/SiO_2(I)$ were coordinated by two phosphines and that of $Rh_4/THP/SiO_2(II)$ was coordinated by one or two phosphines, because the C.N. of Rh–P derived by EXAFS analysis was an averaged value and the number of phosphine ligands coordinated to the Rh_4 cluster were calculated by multiplying the C.N. of Rh–P by four. For example, four Rh atoms of $Rh_4(CO)_8(P(OPh)_3)_4$ were coordinated by four phosphines and the C.N. of Rh–P is 1, and in the case of $Rh_4(CO)_{10}(THP)_2$, two Rh atoms (this means half of the Rh atoms) were coordinated by phosphine ligands and the C.N. should be 0.5.

The C.N.s of Rh–Rh in $Rh_4/THP/SiO_2(I)$ and $Rh_4/THP/SiO_2(II)$ were calculated to be 2.6 and 2.3, respectively, with an error of ±0.1. These results suggested that the Rh_4 framework of the attached Rh_4 clusters on $THP/SiO_2(I)$ remains their cluster framework, because the calculated C.N. was almost 3.

The Rh–P distances of $Rh_4(CO)_{10}(THP)_2$, $Rh_4/THP/SiO_2(I)$, and $Rh_4/THP/SiO_2(II)$ were calculated to be 2.23, 2.28, and 2.23 Å, respectively, with an error of ±0.03 Å.

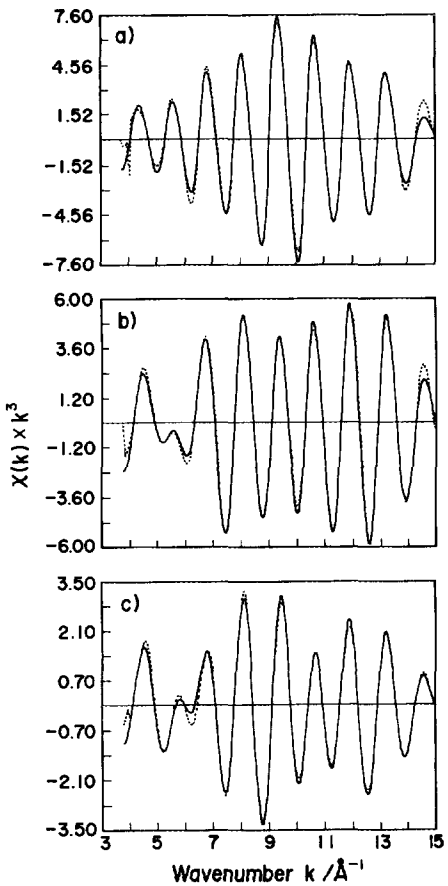

FIG. 4. Inverse Fourier transform of $F(R)$ (plain line) and the curve fitting (dotted line) of (a) $Rh_4(CO)_{12}$, (b) $Rh_4(CO)_8(P(OPh)_3)_4$, (c) $Rh_4/THP/SiO_2(I)$.

TABLE 2

EXAFS Parameters of Rh Carbonyl Clusters in Crystal and Attached on THP/SiO_2[a]

Compound/shell	R (Å)	C.N.	ΔE_0 (eV)	$\Delta\sigma$ (Å)	R factor (%)
$Rh_4(CO)_{12}$					
Rh–Rh	2.73	3.0	7.4	0.034	
Rh–C	1.92	3.8	0.7	0.006	5.8
Rh–O	2.95	3.8	9.7	0.008	
$Rh_6(CO)_{16}$					
Rh–Rh	2.77	4.0	−3.5	0.025	
Rh–C	2.15	5.3	−9.5	0.003	7.5
Rh–O	2.93	5.3	−8.8	0.033	
$Rh_4(CO)_8(P(OPh)_3)_4$					
Rh–Rh	2.73	3.0	0.7	0.030	
Rh–P	2.24	1.0	−1.0	0.047	9.5
Rh–C	1.92	2.8	0.0	0.011	
Rh–O	2.92	2.8	−1.2	0.002	
$Rh_4(CO)_{10}(THP)_2$					
Rh–Rh	2.73	3.0	−3.5	0.033	
Rh–P	2.23	0.44	−8.8	0.007	
Rh–C	1.92	3.3	5.1	0.032	
Rh–O	2.94	3.1	1.4	0.053	8.8
Rh_4/THP/SiO_2(I)					
Rh–Rh	2.76	2.6	3.6	0.072	
Rh–P	2.28	0.56	−3.2	0.000	10.5
Rh–C	1.90	1.9	0.0	0.068	
Rh–O	2.94	1.7	3.6	0.050	
Rh_4/THP/SiO_2(II)					
Rh–Rh	2.74	2.3	7.9	0.068	
Rh–P	2.23	0.30	−6.7	0.000	11.2
Rh–C	1.92	2.9	5.6	0.002	
Rh–O	2.97	1.6	7.1	0.070	

[a] R, C.N., ΔE_0, and $\Delta\sigma$ represent average absorber–backscatterer distance, coordination number, inner potential correction, and difference of the Debye–Waller-like factor from that of reference compounds, respectively.

The Rh–P distance of $Rh_4(CO)_{10}(THP)_2$ and Rh_4/THP/SiO_2(II) were similar to those of $Rh_4(CO)_8(P(OPh)_3)_4$. The Rh–P distance of Rh_4/THP/SiO_2(I) was longer than that of $Rh_4(CO)_{10}(THP)_2$ by 0.05 Å.

The Rh–Rh distance of $Rh_4(CO)_{10}(THP)_2$ was similar to that of $Rh_4(CO)_{12}$ and $Rh_4(CO)_8(P(OPh)_3)_4$. The Rh–Rh distance of Rh_4/THP/SiO_2(I) and Rh_4/THP/SiO_2(II) were calculated to be 2.76 and 2.74 Å, respectively, which were longer than that of $Rh_4(CO)_8(P(OPh)_3)_4$ by 0.03 and 0.01 Å, respectively. However, the difference of 0.03 Å is within the experimental error (±0.02 Å), and it is concluded that the average Rh–Rh distance was almost the same.

On the other hand, the $\Delta\sigma$ of attached Rh_4 clusters was significantly larger than that in crystal. The Rh–Rh $\Delta\sigma$ of $Rh_4(CO)_{12}$, $Rh_4(CO)_8(P(OPh)_3)_4$, and $Rh_4(CO)_{10}(THP)_2$ were calculated to be 0.034, 0.030, and 0.033 Å, respectively. The Rh–Rh $\Delta\sigma$ of Rh_4/THP/SiO_2(I) and Rh_4/THP/SiO_2(II) were calculated to be 0.072 and 0.068 Å, respectively. The error of $\Delta\sigma$ was calculated to be 0.03 Å. Hence, the $\Delta\sigma$ for the Rh–Rh contribution to the attached cluster was larger than that of the Rh_4 clusters in crystal by ca. 0.03 Å. $\Delta\sigma$ represent the distribution of bond distances, when the bond distance was widely distributed $\Delta\sigma$ was increased (22, 23). Thus, the Rh–Rh bond lengths of the attached clusters were distributed more widely than in crystal. This may be caused by the coordination of surface fixed THP ligands, by which the distribution of Rh–Rh distances was increased. As the Rh–Rh distances of the attached Rh_4 clusters were widely distributed, it may possible to represent that the attached Rh_4 clusters on THP/SiO_2(I) was "distorted" by the coordination of surface-fixed THP ligands.

The Rh K-edge XANES (X-ray adsorption near-edge structures) of Rh_4 carbonyl clusters were almost identical, which suggests that the electronic states of the Rh_4 carbonyl clusters are the same.

The lengthening of Rh–P distance and the increase of the Rh–Rh $\Delta\sigma$ contribution is not intrinsic to Rh_4 carbonyl clusters coordinated by THP because the Rh–P distances of $Rh_4(CO)_{10}(THP)_2$ were similar to those of $Rh_4(CO)_8(P(OPh)_3)_4$ and because the Rh–Rh $\Delta\sigma$ of $Rh_4(CO)_{10}(THP)_2$ were similar to those of $Rh_4(CO)_{12}$ and $Rh_4(CO)_8(P(OPh)_3)_4$. If the lengthening of the Rh–P distance and the increase in Rh–Rh $\Delta\sigma$ are intrinsic to Rh_4 carbonyl clusters coordinated by THP, the Rh–P distance and Rh–Rh $\Delta\sigma$ of $Rh_4(CO)_{10}(THP)_2$ should be longer and larger than those of $Rh_4(CO)_{12}$ and $Rh_4(CO)_8(P(OPh)_3)_4$. Hence the lengthening of Rh–P and the increase in Rh–Rh $\Delta\sigma$ are not intrinsic to Rh_4 carbonyl clusters coordinated by THP ligands but appear by the attachment of $Rh_4(CO)_{12}$ on THP/SiO_2(I).

EXAFS analysis showed that $Rh_4(CO)_{12}$ on THP/SiO_2(I) remained in the Rh_4 framework and was coordinated by two THP ligands. The average Rh–P distance and the distribution of Rh–Rh distance were increased by attachment onto a THP-modified SiO_2 surface. The lengthening of the Rh–P distance may be caused by the pulling of two coordinated THPs grafted onto the SiO_2 surface because the average P–P distance between THPs was 8 Å, which is longer than the P–P distance of coordination to Rh_4 clusters on THP/SiO_2(I) by ca. 1.5 Å. As THP is anchored on the SiO_2 surface by the dehydration of one or two OH groups, there is some mobility of the phosphorus atoms of THP. Hence it is possible that two THP coordinate to the Rh_4 clusters and the tension is caused by the distorted THP ligands, as shown in Fig. 6a. It may be difficult for three THP to coordinate to an Rh_4 cluster because the density of THP may be too low to coordinate three THP.

There are two possible explanations for the number of coordinated THPs on Rh_4 clusters. One is that most of the Rh_4 cluster is coordinated by two THPs and the other is that the amount of coordinated THP is distributed from

1 to 3 and the average coordination number is 2. The latter possibility can be excluded because it is unlikely that Rh_4 clusters are coordinated by three THPs, which means the amount of Rh_4 clusters coordinated by one THP ligand is small (even if they exist), while we should remember that the average of the number of the coordinated THPs on Rh_4 cluster is two. Hence, we can conclude that Rh_4 clusters attached on THP/SiO_2(I) are coordinated by two THP ligands homogeneously.

In the case of Rh_4/THP/SiO_2(II), the C.N. of Rh–P was calculated to be 0.30, which suggests that most of the Rh_4 clusters on THP/SiO_2(II) were coordinated by one THP, and some of the Rh_4 clusters were coordinated by two THP. On the IR bands of carbonyl species on Rh_4/THP/SiO_2(II), a small amount of twin CO was observed in addition to the bands of terminal and bridge CO coordinated on phosphine-substituted Rh_4 clusters. This suggest that some of the Rh_4 clusters on THP/SiO_2(II) were decomposed to Rh monomer at room temperature, this is consistent with the C.N. of Rh–Rh being 2.3, which is significantly smaller than 3.0. Clear differences between the wavenumbers of terminal and bridge CO in Rh_4/THP/SiO_2(II) and Rh_4/THP/SiO_2(I) were not observed, which may be due to the broadening of the carbonyl bands of the attached clusters. The Rh_4 cluster on THP/SiO_2(I) was thermally unstable and when the sample was evacuated at 343 K, IR bands corresponding to $Rh_6(CO)_{16}$ and Rh^I monomer appeared at 2080 and 1800 cm^{-1} and 2120 and 2100 cm^{-1}, respectively. Hence, in contrast to the case of Rh_4/THP/SiO_2(I), Rh_4 clusters on Rh_4/THP/SiO_2(II) were not homogeneous. Even though most of the Rh_4 cluster was coordinated by one THP, some part of the Rh_4 cluster was coordinated by two THP ligands and some of the clusters were decomposed to Rh monomer species. The heterogeneity of the Rh clusters/complexes on THP/SiO_2(II) may be caused by the low concentration of THP lingands on the SiO_2 surface and the existence of surface OH groups. The surface density of THP on THP/SiO_2(II) was 0.4 nm^{-2}, which implied that the average distance of THP was 15 Å and the density of the isolated OH that remained was 3.5 nm^{-2}. Hence it is likely that most of Rh_4 was coordinated by one THP because 15 Å was too large to be coordinated by two THP and the distribution of the inter-THP distance caused the Rh_4 clusters coordinated by two THP ligands. The existence of isolated OH groups may cause the decomposition of Rh_4 clusters and cause the decrease of thermal stability.

Figure 5 shows IR spectra of carbonyl ligands of Rh_4/THP/SiO_2(I) evacuated at various temperatures. IR bands of terminal CO were observed at 2064, 2042, and 2022 cm^{-1} and bridge CO was observed at 1870 and 1810 cm^{-1}. When the sample was evacuated below 383 K, peaks at 2064 and 1870 cm^{-1} decreased gradually. When the sample was evacuated at 403 K, the IR band at 1870–1800 cm^{-1} disappeared and the IR band at 2090 cm^{-1} increased. The intensity of these peaks decreased little with evacuation below 353 K.

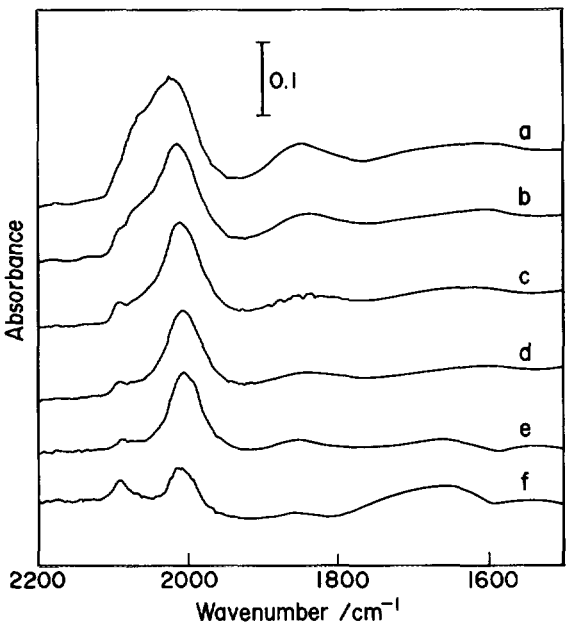

FIG. 5. IR spectra of Rh_4/THP/SiO_2(I). The sample was evacuated at (a) 293 K, (b) 323 K, (c) 343 K, (d) 363 K, (e) 383 K, and (f) 403 K.

An Rh_4 cluster on THP/SiO_2(I) was decomposed gradually by evacuation with increasing temperature as shown in Fig. 5. When the sample was evacuated at 323–383 K the intensities of the IR bands of terminal CO at 2064 and 2042 cm^{-1} and of bridge CO at 1870 cm^{-1} gradually decreased, and the IR band at 2022 cm^{-1} remained at the same intensity. When the sample was evacuated at 403 K, IR bands appeared at 2095 and 2017 cm^{-1}, which can be assigned to twin CO of monometallic species. Hence, the Rh_4 clusters on THP/SiO_2(I) remained in their cluster framework below 383 K even as the coordinated CO was desorbed gradually and converted to rhodium monomer at 403 K. When the sample was heated under CO, the thermal stability was increased and the sample was stable under the reaction condition of hydroformylation. In contrast to the cases of $Rh_4(CO)_{12}$ in solution (20) and impregnated $Rh_4(CO)_{12}$ (14, 15), Rh_4 clusters on THP/SiO_2(I) were not decomposed to $Rh_6(CO)_{16}$ by heat treatment. Aggregation of the Rh_4 clusters to form $Rh_6(CO)_{12}$ is suspended because the Rh_4 cluster on THP/SiO_2(I) was strongly coordinated by THP and the mobility of the rhodium atom may be limited.

Table 3 compares the wavenumbers of CO ligands of tetarhodium carbonyl clusters. The IR bands of coordinated CO of Rh_4/THP/SiO_2(I) are at 2064, 2042 and 2022 cm^{-1} (terminal) and 1870 and 1810 cm^{-1} (bridge). Their wavenumbers are different from those of $Rh_6(CO)_{16}$ (2076,

TABLE 3

Wavenumber of Coordinated CO on Rh Clusters

Compounds	ν(CO)/cm $^{-1}$	
	Linear	Bridge
$Rh_4/THP/SiO_2(I)$	2064, 2042, 2022	1870, 1810
$Rh_4(CO)_{12}/SiO_2$	2080	1800
$Rh_6(CO)_{16}/THP/SiO_2(I)$	2080	1800
$Rh_4(CO)_{12}$[a]	2075, 2047, 2036, 2028	1878, 1870
$Rh_6(CO)_{16}$[a]	2076, 2043	1805
$Rh_4(CO)_{11}PPh_3$[a]	2084, 2057, 2024	1860, 1843
$Rh_4(CO)_{10}(PPh_3)_2$[a]	2067, 2041, 2012	1840, 1818
$Rh_4(CO)_7(PPh_3)_3$[a]	2076, 2049, 2020, 1992	1851, 1827
$Rh_4(CO)_8(PPh_3)_4$[a]	2010, 1995, 1990, 1971, 1965	1793, 1790
$Rh_2(CO)_4Cl_2$[b]	2115, 2095, 2045	

[a] Ref. (42).
[b] Ref. (43).

2043 cm^{-1} (terminal) and 1805 cm^{-1} (bridge)) and $[Rh(CO)_2Cl]_2$ (2115, 2095, and 2045 cm^{-1}), and they are red-shifted from those of $Rh_4(CO)_{12}$ (2075, 2047, 2036, 2028 cm^{-1} (terminal) and 1878, 1870 cm^{-1} (bridge)).

The comparison of carbonyl wavenumbers supported the conclusion from EXAFS analysis that Rh_4 carbonyl clusters on $THP/SiO_2(I)$ remain in their cluster framework and are coordinated by two THP ligands. The IR wavenumbers of the coordinated CO on $Rh_4/THP/SiO_2(I)$ are similar to those of $Rh_4(CO)_{10}(PPh_3)_2$ (2067, 2041, 2012 cm^{-1} (terminal) and 1840, 1818 cm^{-1} (bridge)) and different from those of $Rh_4(CO)_{12}$, $Rh_6(CO)_{16}$, and $[Rh(CO)_2Cl]_2$.

As phosphine ligands donate electrons to Rh atoms, the IR wavenumber of carbonyl ligands coordinated to Rh atoms, which is coordinated by phosphine ligands, is smaller than that of carbonyl ligands on Rh atoms, which is not coordinated by phosphine (28). Hence, in the case of $Rh_4/THP/SiO_2(I)$, the IR bands at 2064, 2042, and 1870 cm^{-1} are assigned to the terminal and bridge CO coordinated to Rh atoms which were coordinated by THP and the IR bands at 2022 and 1810 cm^{-1} are assigned to the terminal and bridge CO on Rh atoms which were not coordinated by THP ligands.

The loading of $Rh_4(CO)_{12}$ was small enough to be anchored on surface-grafted THP ligands. In the case of 4.5 wt% loaded $Rh_4(CO)_{12}$, which was the loading in this work, the surface density of the Rh_4 cluster is 2.2×10^{-1} molecules nm^{-1}, which is about one seventh of the density of THP groups. Hence all Rh_4 clusters can attach to the $THP/SiO_2(I)$ homogeneously.

GC analysis implied that the amount of desorbed CO during attachment of $Rh_4(CO)_{12}$ on $THP/SiO_2(I)$ and $THP/SiO_2(II)$ was 2.8 molecule/1 $Rh_4(CO)_{12}$ cluster and 1.3 molecule/1 $Rh_4(CO)_{12}$ cluster, respectively. About three CO per cluster were desorbed during the impregnation process on $THP/SiO_2(I)$. On the other hand, the number of coordinated THP on the Rh_4 cluster was calculated to be 2 by EXAFS analysis. Hence a coordinative unsaturated site was generated by the attachment process. As shown in Fig. 8 (discussed in a later section), when the fresh $Rh_4/THP/SiO_2(I)$ was exposed to CO, an IR band at 2022 cm^{-1} increased and was assigned to be terminal CO on THP-coordinated Rh atoms. Thus coordinative unsaturated sites may appear on Rh atoms which are coordinated by THP. In the case of $Rh_4/THP/SiO_2(II)$, about one CO per cluster was desorbed during the attachment process. The C.N. of Rh–P calculated by EXAFS analysis was 0.3, which shows that the Rh_4 cluster on $THP/SiO_2(II)$ was coordinated by one THP ligands. Hence, coordination unsaturated site was not generated in the case of $Rh_4/THP/SiO_2(II)$ because the amount of desorbed CO and that of coordinated THP are similar to each other.

Figure 6a shows a proposed structure of attached Rh_4 clusters on $THP/SiO_2(I)$. The Rh_4 framework remains and two Rh atoms (Rh(3) and Rh(4) in the figure) are coordinated by THP and a coordinatively unsaturated site is generated on the THP-coordinating Rh atoms, Rh(3) and Rh(4). The Rh–P distance was lengthened by the pull of surface-anchored THP ligands. The tension from surface-fixed THP ligands caused the distortion of the Rh_4 framework. In the case of $Rh_4/THP/SiO_2$, most of the Rh_4 cluster was coordinated by one THP ligand as shown in Fig. 6b.

3.3. Catalytic Activities Related to the Active Site Structure

Figure 7 shows Arrhenius plots for ethene hydroformylation on $Rh_4/THP/SiO_2(I)$ and $Rh_4/THP/SiO_2(II)$ and on $Rh_6(CO)_{16}$ and $Rh_2(CO)_4Cl_2$ attached on $THP/SiO_2(I)$. The reaction proceeded at 323–368 K under subatmospheric pressure ($p(CO)=p(H_2)=p(C_2H_4)=13.3$ kPa). The turnover frequency (TOF) of propanal formation on the disubstituted Rh_4 cluster by THP ($Rh_4/THP/SiO_2(I)$) was larger than 10^{-2} s^{-1} and the activation energy (E_a) was

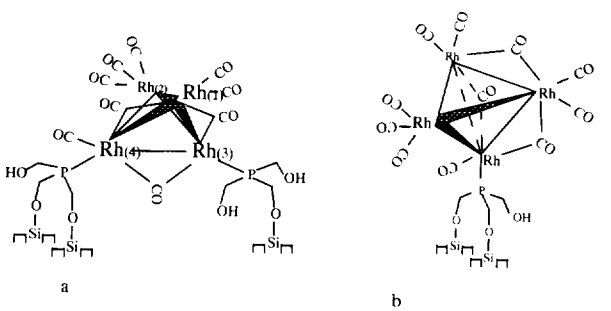

FIG. 6. Proposed structure of attached $Rh_4(CO)_{12}$ on (a) $THP/SiO_2(I)$ and (b) $THP/SiO_2(II)$.

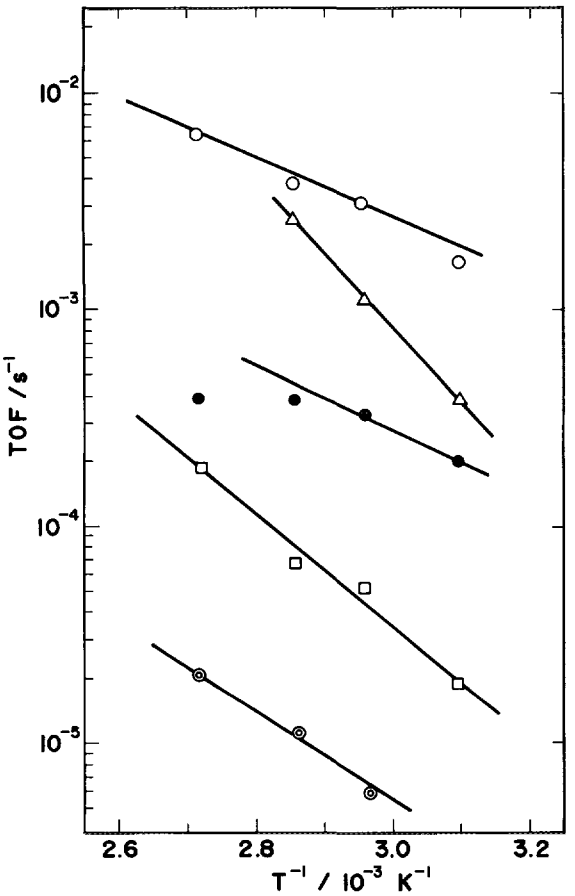

FIG. 7. Arrhenius plots for ethene hydroformylation. Propanal formation rate on (○) $Rh_4/THP/SiO_2(I)$, (△) $Rh_4/THP/SiO_2(II)$, (●) $Rh_2(CO)_4Cl_2$ attached on THP(6.2)/SiO_2, (◎) $Rh_6(CO)_{16}$ attached on $THP/SiO_2(I)$. (□) ethane formation rate on $Rh_4/THP/SiO_2(I)$.

26.5 kJ mol^{-1}. The hydrogenation of ethene proceeded as a side reaction of hydroformylation. The selectivity of propanal was 98% at 368 K and the selectivity of propanal formation increased as the reaction temperatures decreased. The TOF of propanal formation at 338 K on $Rh_2(CO)_4Cl_2$ and $Rh_6(CO)_{12}$ attached on $THP/SiO_2(I)$ was 3.5×10^{-4} and 6×10^{-6} s^{-1}, respectively, values that were one-tenth and one-two-hundredth of that on $Rh_4/THP/SiO_2(I)$. The E_a of propanal formation on $Rh_2(CO)_4Cl_2/THP/SiO_2(I)$ and $Rh_6(CO)_{16}/THP/SiO_2(I)$ were 27.8 and 39.5 kJ mol^{-1}, respectively. The TOFs of propanal formation on the monosubstituted Rh_4 cluster ($Rh_4/THP/SiO_2(II)$) were 2.7×10^{-2} and 3.6×10^{-3} s^{-1} at 353 and 323 K, respectively. $Rh_4/THP/SiO_2(II)$ was thermally unstable and exhibited little catalytic activity below 360 K. The E_a of propanal formation on the monosubstituted Rh_4 cluster ($Rh_4/THP/SiO_2(II)$) was 55.6 kJ mol^{-1}, which was twice as large as that on the disubstituted Rh_4 clusters ($Rh_4/THP/SiO_2(I)$).

The rate of propanal formation on the disubstituted Rh_4 clusters ($Rh_4/THP/SiO_2(I)$) was proportional to $p(CO)^{-0.31}$, $p(H_2)^{1.06}$, and $p(C_2H_4)^{0.29}$. Even under low CO pressure, propanal was produced selectively. The selectivity of aldehyde formation was 93% at 338 K with $p(CO)=1.3$ kPa, $p(H_2)=p(C_2H_4)=13.3$ kPa. Little isotope effect of hydrogen on the reaction rate was observed. The reaction rate in the case of $CO + C_2H_4 + H_2$ was 1.05 times that in the case of $CO + C_2H_4 + D_2$.

Table 4 compares the reaction rate of ethene hydroformylation on the disubstituted Rh_4 clusters ($Rh_4/THP/SiO_2(I)$), $Rh_4(CO)_{10}(THP)_2$, $RhCl(PPh_3)_3$, and $RhH(CO)(PPh_3)_3$. The reactions were carried out at 300 K, $p(CO)=p(C_2H_4)=p(H_2)=33.7$ kPa in tetrahydrofulan (THF) solution. $RhCl(PPh_3)_3$ exhibited no catalytic activity. The TOFs of propanal formation on $Rh_4/THP/SiO_2(I)$, $Rh_4(CO)_{10}(THP)_2$, and $RhH(CO)(PPh_3)_3$ were 4.1×10^{-8}, 1.4×10^{-9}, and 8.8×10^{-8} s^{-1}, respectively. The reaction rate on the surface-anchored disubstituted cluster ($Rh_4/THP/SiO_2(I)$) was 30 times that on $Rh_4(CO)_{10}(THP)_2$ and was of the same magnitude as that of $RhH(CO)(PPh_3)_3$. Leaching of rhodium from $Rh_4/THP/SiO_2(I)$ is not observed during the hydroformylation reaction suspended in THF.

Propene hydroformylation also proceeded on the disubstituted cluster ($Rh_4/THP/SiO_2(I)$) at 333 K with $p(CO)=p(H_2)=p(C_3H_6)=13.3$ kPa. The normal/iso ratio of butanal was 1.0. This reaction also proceeded on $RhH(CO)(PPh_3)_3$ at 300 K with $p(CO)=p(H_2)=p(C_3H_6)=33.7$ kPa in THF solution. The normal/iso ratio of butanal was 3.0 in this case.

As shown in Fig. 7, $Rh_4/THP/SiO_2(I)$ is an active catalyst for olefin hydroformylation. The catalytic reaction proceeded below 323 K and the selectivity of propanal formation was more than 98%. The activation energy was 26.5 kJ mol^{-1}. The reaction rate of ethene hydroformylation is much higher than that of other attached Rh clusters, an activity level equal to that of a Wilkinson complex, as

TABLE 4

Reaction Rate of Ethylene Hydroformylation[a] over $Rh_4/THP/SiO_2(I)$, $Rh_4(CO)_{10}(THP)_2$, $RhCl(PPh_3)_3$, and $RhH(CO)(PPh_3)_3$ in THF

Catalyst (in THF solution)	TOF/s^{-1}
$Rh_4/THP/SiO_2(I)$	4.1×10^{-8}
$Rh_4(CO)_{10}(THP)_2$	1.4×10^{-9}
$RhCl(PPh_3)_3$	0.0
$RhH(CO)(PPh_3)_3$	8.8×10^{-8}

[a] $T = 300$ K; $p(H_2) = p(CO) = p(C_2H_4) = 33.7$ kPa.

shown in Table 4. Iwasawa *et al.* reported the reaction rate of ethene hydroformylation on attached Rh dimer (10) and Se-doped Rh_6 carbonyl clusters (29). The turnover frequencies of ethene hydroformylation on the Rh dimer and Rh_6 were reported to be 5×10^{-5} s^{-1} (413 K; total pressure, 40.0 kPa; $H_2:CO:C_2H_4 = 1:1:1$) and 1×10^{-3} s^{-1} (398 K; total pressure, 40.0 kPa; $H_2:CO:C_2H_4 = 1:1:1$). The turnover frequency on $Rh_4/THP/SiO_2(I)$ was larger than that on the Rh dimer and The Se-doped Rh_6 clusters even when the reaction temperature was lower, TOF = 6×10^{-3} s^{-1} (368 K, total pressure, 40.0 kPa; $H_2:CO/C_2H_4 = 1:1:1$). Besides, $Rh_4/THP/SiO_2(I)$ was much more active for ethene hydroformylation than $Rh_2(CO)_4Cl_2$ and $Rh_6(CO)_{16}$ attached on $THP/SiO_2(I)$. This large difference in activity also supported the proposal that Rh_4 carbonyl clusters were not decomposed to $Rh_6(CO)_{16}$ or monometallic species. If the catalytic active sites were not Rh_4 clusters to $THP/SiO_2(I)$ and a minor Rh species which was not observed by IR measurement, the TOF of hydroformylation on the minor species should be at least ca. 10 times as large as that of Wilkinson complexes, which are some of the most active catalysts for hydroformylation. Because we can observe the IR bands of the minor species when the proportion of the species is larger than 0.1, this possibility may be much smaller than the possibility that the Rh_4 clusters that were coordinated by two THPs, the major species on $THP/SiO_2(I)$, were the active site for hydroformylation reaction.

In homogeneous Rh catalysts, $Rh_4(CO)_{12}$ is sometimes used as a precursor of the catalyst (30–32). Under catalytic reaction conditions, however, $Rh_4(CO)_{12}$ were decomposed to Rh monomer and the reaction proceeded on the monomer species in most cases; only in a few instances does the literature say that Rh_4 remains in the cluster structure under reaction conditions, without spectroscopic evidence (33).

The distortion of Rh_4 clusters is an essential factor for active and selective hydroformylation because the distorted Rh_4 cluster ($Rh_4/THP/SiO_2(I)$) is much more active than the undistorted Rh_4 clusters ($Rh_4/THP/SiO_2(II)$ and $Rh_4(CO)_{10}(THP)_2$). As discussed in the previous section, Rh_4 clusters attached to $THP/SiO_2(I)$ were distorted by the coordination of two THP ligands, where the Rh–P distance was lengthened by 0.04 Å and the Rh–Rh $\Delta\sigma$ was increased to 0072 Å. In contrast, the Rh–P distance and the Rh–Rh $\Delta\sigma$ of $Rh_4/THP/SiO_2(II)$ and $Rh_4(CO)_{10}(THP)_2$ were similar to those of $Rh_4(CO)_{12}$ and $Rh_4(CO)_8(P(OPh)_3)_4$. The large difference in activity between the former and the latter is shown in Fig. 7 and Table 4. The activation energy on $Rh_4/THP/SiO_2(I)$ (26.5 kJ mol^{-1}) was half that on $Rh_4/THP/SiO_2(II)$ (55.6 kJ mol^{-1}). The TOF of $Rh_4/THP/SiO_2(I)$ suspended in THF was 4.1×10^{-8} s^{-1}, which was 30 times larger than that of $Rh_4(CO)_{10}(THP)_2$ in THF solution (1.4×10^{-9} s^{-1}). The electronic states of

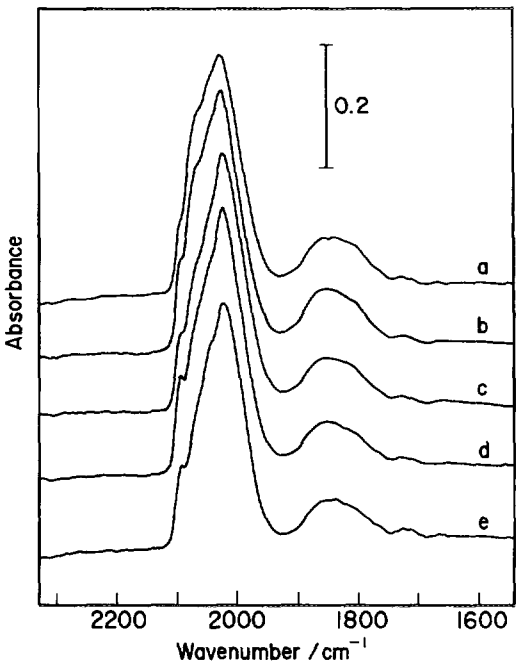

FIG. 8. IR spectra of $Rh_4/THP/SiO_2(I)$. (a) Evacuated 300 K; (b) exposed to CO at 300 K; (c) after (b), exposed to C_2H_4 at 298 K; (d) after (c), exposed to CO at 298 K; and (e) after (d), exposed to CO at 338 K.

$Rh_4/THP/SiO_2(I)$ and $Rh_4(CO)_{10}(THP)_2$ should be almost the same, because the Rh_4 clusters of both are coordinated by two THP ligands and we did not observe any difference in Rh K-edge XANES (X-ray adsorption near-edge structure) between $Rh_4/THP/SiO_2(I)$ and $Rh_4(CO)_{10}(THP)_2$. The difference between them is due to the distortion of the Rh_4 framework. The distorted Rh_4 clusters ($Rh_4/THP/SiO_2(I)$) were more active than normal Rh_4 clusters ($Rh_4/THP/SiO_2(II)$ and $Rh_4(CO)_{10}(THP)_2$). Hence we can conclude that the distortion of the Rh_4 framework is one of the essential factors for active and selective hydroformylation.

Several studies have been performed regarding the relation between cluster structure and catalytic activities (1–5, 34). They said that metal clusters with an open structure (the so-called "butterfly structure") are more active than those with closed structures in general. Sometimes, however, it is difficult to separate structural effects from electronic effects because they are strongly related each other. The results presented in this paper clearly show that a small difference in structure can strongly affect the reactivity.

3.4. Dynamic Behavior of Attached Rh_4 Clusters under Reaction Conditions and Reaction Mechanisms

Figure 8 shows IR spectra of $Rh_4/THP/SiO_2(I)$ after exposure to CO and C_2H_4. When the sample was exposed to CO the IR bands at 2022 cm^{-1} increased. The intensity of these IR bands decreased to original intensity with evac-

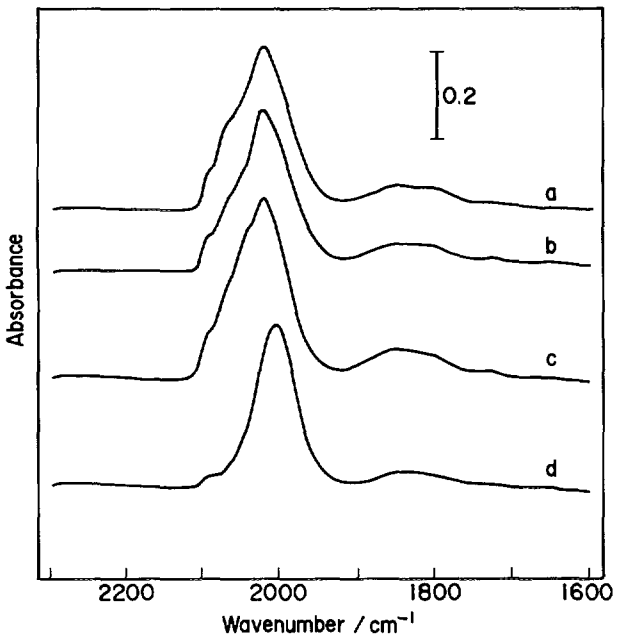

FIG. 9. IR spectra of $Rh_4/THP/SiO_2(I)$. (a) Evacuated 300 K; (b) exposed to C_2H_4 at 300 K after (a); (c) exposed to CO at 338 K after (b); (d) exposed to H_2 + C_2H_4 at 298 K after (c).

TABLE 5

EXAFS Parameters of $Rh_4/THP/SiO_2(I)$ in the Presence of Various Gases[a]

Compound/shell	R (Å)	C.N.	ΔE_0 (eV)	$\Delta\sigma$ (Å)	R factor (%)
(a) $Rh_4/THP/SiO_2(I)$ (vac.)					
Rh–Rh	2.76	2.6	3.6	0.072	
Rh–P	2.28	0.56	−3.2	0.000	10.5
Rh–C	1.90	1.9	0.0	0.068	
Rh–O	2.94	1.7	3.6	0.050	
(b) $Rh_4/THP/SiO_2(I)$ (exposed to C_2H_4 followed by evac.)					
Rh–Rh	2.76	2.4	0.7	0.072	
Rh–P	2.28	0.58	−4.7	0.001	11.6
Rh–C	1.92	1.0	−0.0	0.068	
Rh–O	2.92	0.95	5.6	0.050	
(c) $Rh_4/THP/SiO_2(I)$ (after (b), exposed to CO at 300 K)					
Rh–Rh	2.76	2.5	2.2	0.070	
Rh–P	2.28	0.50	−2.5	0.003	8.7
Rh–C	1.91	1.1	1.4	0.068	
Rh–O	2.93	1.0	−2.1	0.042	
(d) $Rh_4/THP/SiO_2(I)$ (after (c), exposed to CO at 338 K)					
Rh–Rh	2.76	2.4	3.7	0.072	
Rh–P	2.28	0.58	−1.8	0.008	9.9
Rh–C	1.91	1.9	1.5	0.068	
Rh–O	2.93	1.7	2.2	0.040	

[a] Notation as in Table 2.

uation at 300 K. When the sample was exposed to ethene IR bands at 2064, 2042, and 1870 cm^{-1} decreased and the intensity of these bands increased when the sample was exposed to CO at 338 K. When the sample was exposed to hydrogen, a tendency similar to the case of exposure to ethene was observed; the IR bands at 2064 and 2042 cm^{-1} decreased in intensity.

Figure 9 shows the IR spectra of $Rh_4/THP/SiO_2(I)$ after exposure to reactant gases. When the sample was exposed to ethene, IR bands at 2064, 2042, and 1870 cm^{-1} decreased, similarly to the bands in Fig. 8. The intensity of these bands increased to original intensity when the sample was exposed to reactant gases of ethene hydroformylation at 338 K ($p(CO)=p(H_2)=p(C_2H_4)=13.3$ kPa) followed by exposure to ethene. After that, when the sample was exposed to reactant gases of ethene hydrogenation ($p(H_2)=p(C_2H_4)=13.3$ kPa) at 300 K, IR bands of terminal CO at 2064, 2042 cm^{-1} disappeared and the IR band at 2022 cm^{-1} red-shifted toward 2005 cm^{-1} under the reaction conditions of hydrogenation.

Table 5 shows structural parameters of $Rh_4/THP/SiO_2(I)$ in the presence of various gases. The C.N. and the Rh–Rh and Rh–P distances of $Rh_4/THP/SiO_2(I)$ did not change after hydroformylation and hydrogenation reaction. The coordination numbers for Rh–C and Rh–O were influenced by the gas phase. Other parameters, however, remained unchanged in the presence of reactant gases of hydroformylation. When the $Rh_4/THP/SiO_2(I)$ was exposed to C_2H_4, the C.N.'s of Rh–C and Rh–O decreased to 1.0 and 0.95, respectively. After that, when CO was admitted into the sample at 300 K, the C.N.s of Rh–C and Rh–O remained at almost the same value, the C.N.'s of Rh–C and Rh–O being 1.1 and 1.0, respectively. When the sample was exposed to CO at 338 K, the C.N.s of Rh–C and Rh–O increased and returned to their initial values, the C.N.s of Rh–C and Rh–O being 1.9 and 1.7, respectively.

Figure 10 shows the produced amounts of propanal and ethane as functions of reaction period. On fresh $Rh_4/THP/SiO_2(I)$, propanal was produced linearly from the initial stage of the reaction and the selectivity of propanal formation was more than 98%. On the other hand, when $Rh_4/THP/SiO_2(I)$ was exposed to C_2H_4 before reaction the formation rate of ethane was about three times higher than that of the fresh catalyst and the rate of propanal formation was about half that of the fresh catalyst at the initial stage (before 10 min). In the steady state (after 10 min), the rates of propanal and ethane formation were the same as on the fresh catalyst.

Figure 11 shows the amount of ethane produced as a function of reaction period. The reaction was carried out at 254 K, $p(H_2)=p(C_2H_4)=13.3$ kPa. For fresh $Rh_4/THP/SiO_2(I)$, an induction period was observed. The reaction rate gradually increased for 20 min and then reached a constant value. The induction period was not observed

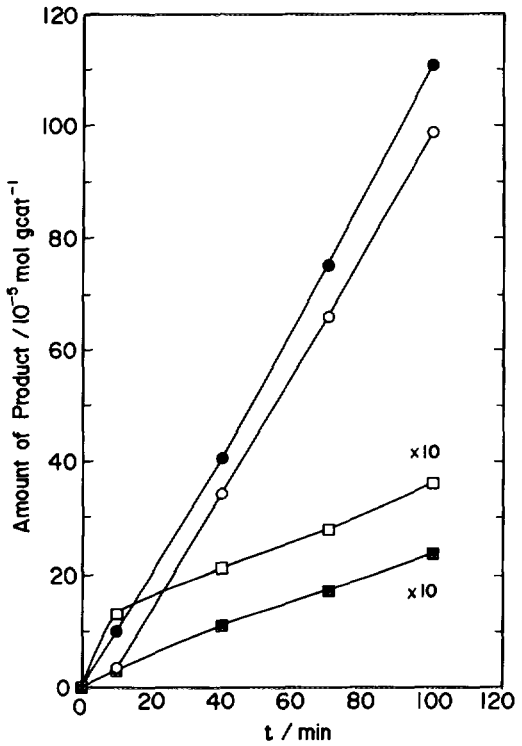

FIG. 10. Amount of products as a function of reaction period. Propanol formation on (●) fresh $Rh_4/THP/SiO_2(I)$ and (○) $Rh_4/THP/SiO_2(I)$ exposed to C_2H_4 before reaction. Ethane formation on (■) fresh catalyst and (□) the catalyst exposed to ethene before reaction. $p(CO) = p(H_2) = p(C_2H_4) = 13.3$ kPa; $T = 338$ K.

after a second run when the catalyst was preexposed to C_2H_4 at 300 K before reaction. The induction period was observed again when the catalyst which was used in a second run and exposed to ethene was exposed to CO at 338 K. When the catalyst was exposed to ethene before reaction the induction period was not observed. The steady state reaction rate was not changed by these treatments.

As shown in Figs. 8 and 9, IR results suggested that CO ligands desorbed and coordinated to the Rh_4 cluster reversibly under reaction conditions. When the sample was exposed to CO the bands at 2022 cm^{-1} increased and their intensity decreased reversibly by the evacuation. When the sample was exposed to C_2H_4, the IR bands at 2064, 2042, and 1870 cm^{-1} were decreased and did not increase with evacuation or exposure to CO at room temperature. The band intensity at 2064, 2042, and 1870 cm^{-1} was increased by exposure to CO at 338 K. These changes induced by the gas phase were reversible; IR bands at 2064 and 2042 cm^{-1} were decreased by exposure to ethene at 300 K and the intensity increased again with exposure to CO at 338 K.

From Fig. 8 and the previous assignment, the influence of the reactant on the CO ligand can be described as follows. When the $Rh_4/THP/SiO_2(I)$ was exposed to ethene, the coordinated carbonyl on Rh(1) and Rh(2) in Fig. 6 desorbed and they coordinated reversibly by the admission to CO at 338 K. EXAFS analysis supported this idea. The C.N.'s of Rh–C and Rh–O decreased with exposure to ethene at room temperature and increased again with exposure to CO at 338 K. The distances and C.N.'s of Rh–Rh and Rh–P were not affected by exposure to the reactant gases, which suggested that the structure of the Rh_4 framework was not affected by the gas phase.

The change in coordinated carbonyl was also observed under reaction conditions of hydroformylation and hydrogenation, as shown in Fig. 9. Under reaction conditions of hydroformylation all Rh atoms of $Rh_4/THP/SiO_2(I)$ are coordinated by CO because IR bands of terminal and bridge CO coordinating to all Rh atoms of the clusters were observed (Fig. 9c); under reaction conditions of hydrogenation the coordinated CO on Rh(1) and Rh(2) in Fig. 6 is desorbed because IR bands at 2064, 2042, and 1870 cm^{-1} disappeared. Even when the catalyst was preexposed to ethene, the IR intensity of the bands at 2064 and 2042 cm^{-1} reversibly increased under the reaction conditions of hydroformylation, as shown in Figs. 9b and 9c.

Figure 12 shows the proposed structure of $Rh_4/THP/SiO_2(I)$ affected by the gas phase. Under CO and under reaction conditions of hydroformylation, the Rh atoms

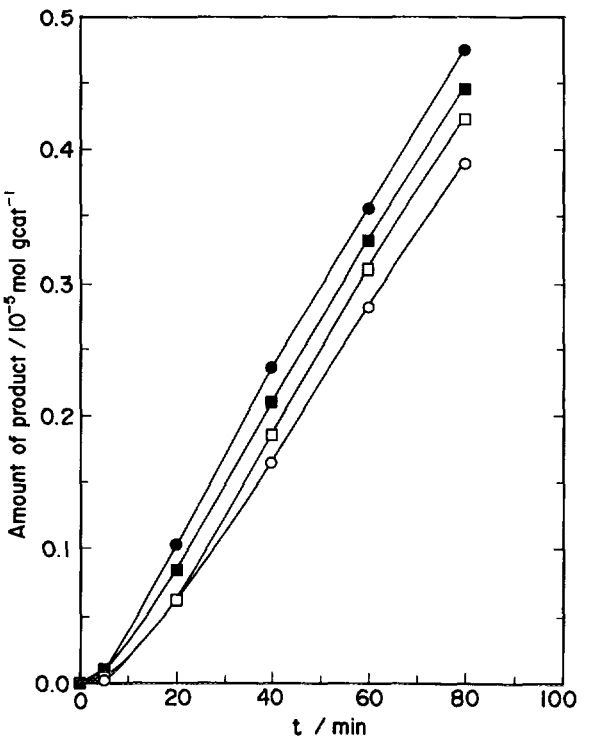

FIG. 11. Amount of ethane formation as a function of reaction period on $Rh_4/THP/SiO_2(I)$. (○) first run; (●) second run; (□) after second run, the catalyst was exposed to CO at 338 K before reaction; (■) catalyst was exposed to C_2H_4 before reaction.

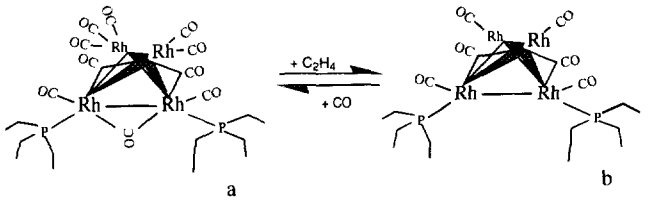

FIG. 12. Proposed structure of transformation of Rh_4 clusters on $Rh_4/THPSiO_2(I)$ (a) in the presence of CO and (b) in the presence of ethene.

were coordinated by CO (Fig. 12a). On the other hand, under C_2H_4 and H_2, and under reaction conditions of hydrogenation, CO ligands were desorbed (Fig. 12b). The Rh_4 framework was little influenced by the gas phase because the distances and C.N.s of Rh–Rh and Rh–P remained unchanged in the presence of reactant gases.

The reaction rate and selectivity are affected by the state of coordinated carbonyl species. Results in Figs. 10 and 11 suggested that structure a in Fig. 12 is active for hydroformylation and inactive for hydrogenation. In contrast, structure b in Fig. 12 is active for hydrogenation and inactive for hydroformylation. As shown in Fig. 10, propanal was produced linearly from the initial stage of hydroformylation reaction when fresh $Rh_4/THP/SiO_2(I)$ was used as a catalyst. On the other hand, an induction period was observed when $Rh_4/THP/SiO_2(I)$ which had been preexposed to ethene was used as catalyst. At the initial stage of the reaction, ethane was produced quickly and the rate of propanal formation was low. The steady state reaction rates were almost equal. As mentioned previously, when the catalysts were exposed to ethene, they had structure b in Fig. 12 and converted to structure a under the reaction conditions of hydroformylation as shown in Figs. 9b and 9c. Hence, structure b is inactive for hydroformylation and the activity was brought about by the conversion of active sites toward structure a in Fig. 12. In contrast, in the case of hydrogenation, an induction period was observed when fresh catalyst or catalyst preexposed to CO was used, and little induction period was observed in the second run and in the case of the catalyst preexposed to ethene. The steady state reaction rates were similar to each other. The fresh catalyst and the catalyst in the presence of CO have structure a in Fig. 12 and the catalyst under hydrogenation reaction and in the presence of ethene have structure b as shown in Figs. 8 and 9. Hence, structure b is the active species for hydrogenation and structure a is inactive for this reaction. The catalytic activity is generated by the conversion of the active site structure toward structure b. Thus it is concluded that high selectivity of the hydroformylation reaction toward aldehyde was achieved by the dynamic transformation of the active site structure. Structure a in Fig. 12 is active for hydroformylation and structure b is inactive for this reaction, and the active site structure was converted to structure a under the reaction conditions of hydroformylation. On the other hand, structure b is active for hydrogenation and structure a is inactive, and the active site structure is converted to structure b under the reaction conditions of hydrogenation.

The reaction site of hydroformylation may be Rh(3) and Rh(4) in Fig. 6, because Rh(1) and Rh(2) of $Rh_4/THP/SiO_2(I)$ were coordinated by CO under reaction conditions of hydroformylation and ethene cannot coordinate the upper Rh atoms. Hence, ethene may coordinate to Rh(3) and Rh(4) in Fig. 6 and the reaction site of hydroformylation may be Rh(3) and Rh(4) of $Rh_4/THP/SiO_2(I)$. Under the reaction conditions of hydroformylation, even Rh(3) and Rh(4) may be weakly blocked by CO because the reaction rate is proportional to $p(CO)^{-0.31}$. Ethene can adsorb relatively strongly on the active site and the adsorption of hydrogen should be weak because the reaction rate is proportional to $p(C_2H_4)^{0.29}$ and $p(H_2)^{1.06}$. Under the reaction conditions of hydrogenation, all Rh atoms of $Rh_4/THP/SiO_2(I)$ were coordinately unsaturated and all Rh atoms could act as active sites. This form is suitable for hydrogenation because an ensemble of metal atoms is needed to coadsorb ethene and hydrogen. The dependence on the pressure of the reactants was similar to that on Wilkinson complexes (35).

Rosas *et al.* investigate the hydroformylation of cyclohexene on $Rh_4(CO)_{12}$ in solution and they proposed a reaction mechanism involving the reversible cleavage of Rh–Rh bonds by coordination with hydrogen (33). While the reversible cleavage of Rh–Rh bonds by the reactant of hydroformylation was not detected by EXAFS measurement in the case of $Rh_4/THP/SiO_2(I)$, this may be because of the low concentration of the cleaved Rh clusters.

$Rh_4/THP/SiO_2(I)$ exhibits activity similar to that of $RhH(CO)(PPh_3)_3$, which is one of the most active catalysts for hydroformylation in solution (36, 37). We should recall that TOF is calculated by dividing the total moles of Rh atoms into the reaction rate and that only Rh(3) and Rh(4) act as active sites. Thus, the real TOF on $Rh_4/THP/SiO_2(I)$ is as high as on Wilkinson complexes. Catalytic performance in terms of the regio selectivity is, however, slightly different. The normal/iso ratio of butanal on $Rh_4/THP/SiO_2(I)$ was 1.0 and that on $RhH(CO)(PPh_3)_3$ was 3.0. An activation barrier to the oxidative addition of hydrogen exists in Wilkinson complexes (35, 38). In $Rh_4/THP/SiO_2(I)$, the activation barrier to oxidative addition of hydrogen does not exist because little isotope effect was observed on H_2. The activation barrier on $Rh_4/THP/SiO_2(I)$ should exist at the step which did not contain movement of hydrogen atoms such as CO insertion.

CONCLUSIONS

(1) THP was anchored on the SiO_2 surface, designated as THF/SiO_2 by dehydration with surface OH groups.

(2) $Rh_4(CO)_{12}$ was coordinated with THP/SiO_2 by phosphin substitution while remaining in the Rh_4 framework.

(3) The attached structure of Rh_4 carbonyl clusters was dependent on the loading of THP. In the case of Rh_4/THP (6.2wt% THP loading)/SiO_2(I), Rh_4 clusters were coordinated by two THPs anchored on SiO_2, whereas for Rh_4/THP (1.0wt% THP loading)/SiO_2(II), Rh_4 clusters were coordinated by one THP anchored on $SiO_2P(CH_2OH)_{3-x}(CH_2O)_x (x = 1–2)$.

(4) Rh_4 clusters on Rh_4/THP/SiO_2(I) were found by EXAFS evaluation to be distorted and Rh–P distances was considerably lengthened compared with $Rh_4(CO)_8(P(Oph)_3)_4$ and $Rh_4(CO)_{10}(THP)_2$.

(5) Rh_4/THP/SiO_2(I) was catalytically active and selective for olefin hydroformylation reaction toward aldehydes, comparable to Wilkinson complex $RhH(CO)(PPh_3)_3$ in solution.

(6) The distortion of Rh_4 clusters on Rh_4/THP/SiO_2(I) is proposed to be associated with their higher activities and selectivities for olefin hydroformylation reaction, compared with Rh_4/THP/SiO_2(II) or $Rh_4(CO)_{10}(THP)_2$ in solution.

(7) CO ligands bound with Rh_4 moiety in the Rh_4/THP/SiO_2(I) are reversibly eliminated under catalytic reaction conditions, which cause selective hydroformylation of olefin.

ACKNOWLEDGMENTS

The authors acknowledge Professor Nomura and the PF staff for their technical assistance in measuring EXAFS spectroscopy. The EXAFS experiments were carried out under the approval of the EXAFS Program Committee (Proposal No. 92004). The authors acknowledge Mr. Nagata and Mr. Kasano, Polymer Reserach Laboratory, TOSOH Corporation, for the quantitative analysis of phosphorous contents in the samples by XPS.

REFERENCES

1. Ichikawa, M., *in* "Tailored Metal Catalysis" (Y. Iwasawa, Ed.), p. 138, Reidel, Dordrecht, 1984; *Polyhedron* **7,** 2351 (1988).
2. Ichikawa, M., *Adv. Catal.* **38,** 283 (1992).
3. Iwasawa, Y., *Adv. Catal.* **35,** 187 (1987).
4. Gates, B. C., Guczi, L., and Knozinger, H., Eds., "Metal Clusters in Catalysis." Elsevier, Amsterdam, 1986.
5. Gates, B. C., *in* "Metal Clusters" (M. Moskovits, Ed.), p. 283. Wiley, New York, 1986.
6. Ichikawa, M., Rao, L. F., Kimura, T., and Fukuoka, A., *J. Mol. Catal.* **62,** 15 (1990).
7. Rao, L. F., Fukuoka, A., Kosugi, N., Kuroda, H., and Ichikawa, M., *J. Phys. Chem.* **94,** 5317 (1990).
8. Fukuoka, A., Kimura, T., Kosugi, N., Kuroda, H., Minai, Y., Sakai, Y., Tominaga, T., and Ichikawa, M., *J. Catal.* **126,** 434 (1990).
9. Iwasawa, Y., Asakura, K., Ishii, H., and Kuroda, H., *Z. Phys. Chem.* **144,** 105 (1985).
10. Asakura, K., Bando, K. K., Iwasawa, Y., Arakawa H., and Isobe, K., *J. Am. Chem. Soc.* **112,** 9096 (1990); *J. Am. Chem. Soc.* **112,** 3242 (1990).
11. Iwasawsa, Y., "Tailored Metal Catalysis" (Y. Iwasawa, Ed.), p. 1. Reidel, Dordrecht, 1984.
12. Psaro, R., and Ugo, R., *in* "Metal Clusters in Catalysis" (B. C. Gates, L. Guczi, and L. Knozinger, Eds.). Elsevier, Amsterdam, 1986.
13. Hogde, P., and Sherrington, D. C., eds.), "Polymer-Supported Reactions in Organic Synthesis." Wiley, Chichester/New York, 1980.
14. Theolier, A., Smith, A. K., Leconte, M., Basset, J. M., Zanderight, G. M., Psaro, P., and Ugo, R., *J. Organomet. Chem.* **191,** 415 (1980).
15. Rode, J. E., Davis, M. E., and Hanson, B. E., *J. Catal.* **96,** 574 (1985).
16. Shido, T., Okazaki, T., Ulla, M. A., Fujimoto, T., and Ichikawa, M., *Catal. Lett.* **20,** 37 (1993).
17. Shido, T., Okazaki, T., and Ichikawa, M., *Catal. Lett.* **17,** 97 (1993).
18. Coskran, K. J., and Verkade, J. G., *Inorg. Chem.* **4,** 1655 (1965).
19. Martinengo, S., Chini, P., and Giordano, G., *J. Organomet. Chem.* **27,** 389 (1971).
20. Chini, P., and Martinengo, S., *Inorg. Chim. Acta* **3,** 315 (1969).
21. Kosugi, N., and Kuroda, H., "Program EXAFS2." Research Center for Spectrochemistry, The University of Tokyo, 1988.
22. Teo, B. K., "EXAFS: Basic Principles and Data Analysis." Springer-Verlag, Berlin, 1986.
23. Koningsberger, D. C., and Prins, R., Eds., "X-ray Adsorption." Wiley-Interscience, New York, 1988.
24. Wei, C. H., and Dahl, L. F., *J. Am. Chem. Soc.* **91,** 1351 (1969).
25. Wei, C. H., *Inorg. Chem.* **8,** 2384 (1969).
26. Corey, E. R., Dahl, L. F., and Beck, W., *J. Am. Chem. Soc.* **85,** 1202 (1963).
27. Ciani, G., Garlaschelli, L., Manassero, M., and Sartorelli, U., *J. Organomet. Chem.* **129,** C25 (1977).
28. Yamamoto, A., "Organotransition Metal Chemistry." Wiley–Interscience, New York (1986).
29. Izumi, Y., and Iwasawa, Y., *J. Phys. Chem.* **96,** 10942 (1992)).
30. Castells, J., Merino, M. A., and Moreno-Manas, M., *J. Chem. Soc. Chem. Commun.*, 709 (1972).
31. Heil, B., and Marko, L., *Chem. Ber.* **101,** 2209 (1968).
32. Lazzaroni, R., Pertici, P., Bertozzi, S., and Fabrizi, G., *J. Mol. Catal.* **58,** 75 (1990).
33. Rosas, N., Marquez, C., Hernandez, H., and Gomez, R., *J. Mol. Catal.* **48,** 59 (1988).
34. Suss-Fink, G., and Meister, G., *Adv. Orgamomet. Chem.* **35,** 41 (1993).
35. Divekar, S. S., Deshpande, R. M., and Chaudhari, R. V., *Catal. Lett.* **21,** 191 (1993).
36. Cornils, B., *in* "New Synthesis with Carbon Monoxide" (T. Falbe, Ed.). Springer, Berlin, 1980.
37. Parshall, G. W., and Ittel, S. D., "Homogeneous Catalysis: The Applications and Chemistry of Catalysis by Soluble Metal Complexes." Wiley, New York, 1992.
38. Deshpande, R. M., and Chaudhari, R. V., *J. Catal.* **115,** 326 (1989).
39. Wyckoff, P. W. G., "Crystal Structures," Vol. 1. Interscience, New York, 1948.
40. LaPlaca, S. J., and Ibers, J. A., *Acta Crystallogr.* **18,** 511 (1965).
41. Wells, A. F., "Structural Inorganic Chemistry," p. 959. Clardendon, Oxford, 1984.
42. Whyman, R., *J. Chem. Soc. Dalton Trans.*, 1375 (1972).
43. Colton, R., Farthing, R. H., and Knapp, J. E., *Aust. J. Chem.* **23,** 1351 (1970).